Dalton Transactions

Accepted Manuscript

ROYAL SOCIETY OF CHEMISTRY

www.rsc.org/dalton

Journal Name

RSCPublishing

ARTICLE

Single-molecule magnet behavior in three cyano-bridged heterometallic Fe^{III}–Ni^{II} clusters

Cite this: DOI: 10.1039/x0xx00000x

Peng-Fei Zhuang,[a] Yan-Juan Zhang,[a] Hui Zheng,[a] Cheng-Qi Jiao,[a] Liang Zhao,[a] Jun-Li Wang,[a] Cheng He,[a] and Chun-Ying Duan,[a] Tao Liu,*[a]

Received 00th January 2012,
Accepted 00th January 2012

DOI: 10.1039/x0xx00000x

www.rsc.org/

One trinuclear and two tetranuclear cyanide-bridged Fe^{III}–Ni^{II} complexes were synthesized via treatment of tricyanometallate with divalent Ni salts in the presence of 1-butylimidazole, 2,2-bipyrimidyl and 1,10-phenanthroline, respectively. Magnetic property studies demonstrated that the three complexes exhibit single-molecule magnet behavior as a result of strong intracluster ferromagnetic coupling and weak intercluster magnetic interactions.

Introduction

The design and synthesis of single-molecule magnets (SMMs), exhibiting slow magnetic relaxation, have attracted extensive attention due to their potential applications in high-density information storage and quantum computation.[1] Up to date, various strategies have been reported to obtain SMMs. Among them, one efficient synthetic approach is to utilize metallocyanates building blocks as multidentate ligands and linkers. The cyano group can efficiently transmit magnetic interactions between multifarious transition-metal ions.[2] Additionally, the linear bridging mode of the cyano group enables chemists to reasonably predict the nature of the exchange interactions in some cases.[3] Therefore, metallocyanates building blocks have been extensive employed. Among them, the use of $[Fe^{III}L(CN)_3]^-$ (L = tridentate ligand) as metallocyanates building block has produced various discrete polynuclear complexes and 1D assemblies, and some of them are promising SMMs.[4] Moreover, the presence of the intermolecular magnetic interactions, even if very weak, is supposed to suppress the slow relaxation of SMMs. One efficient approach to decrease the intermolecular magnetic interactions is to enhance the steric hindrance by introducing bulky building blocks and ancillary ligands into the molecules.[5] Based on the above strategy, we choose the bulky $[Fe^{III}L(CN)_3]^-$ as the building block, and the bulky 1-butylimidazole, 2,2-bipyrimidyl and 1,10-phenanthroline were adopted as ancillary ligands. With a rational design, we succeeded in synthesizing three new cyano-bridged heterometallic Fe^{III}–Ni^{II} clusters: $[(pzTp)Fe^{III}(CN)_3]_2Ni^{II}$(1-butylimidazole)$_4\cdot CH_3OH$ (PzTp = tetrakis(pyrazolyl)borate) (**1**), $[(Tp^*)Fe^{III}(CN)_3]_2Ni^{II}_2$(2,2-bipyrimidyl)$_4\cdot 2BF_4\cdot 2CH_3OH\cdot 2H_2O$ (Tp* = hydrotris(3,5-dimethylpyrazolyl)borate) (**2**) and $[(Tp)Fe^{III}(CN)_3]_2Ni^{II}_2$(1,10-phenanthroline)$_4\cdot 2ClO_4\cdot 2H_2O$ (Tp = (hydrotris(pyrazolyl)borate) (**3**). Herein, we reported the synthesis, single crystal structures, and SMM behavior of complexes **1**–**3**.

Results and discussion

Crystal structure of complexes 1-3

Complex **1** was synthesized by a diffusion method in a test tube. Single-crystal X-ray diffraction analyses revealed that **1** crystallized in the triclinic space group $P\bar{1}$. The crystal structure consists of neutral $[Fe^{III}(pzTp)(CN)_3]_2Ni^{II}$(1-butylimidazole)$_4$ clusters and uncoordinated methanol molecules located between the clusters. In the trinuclear cluster, the $[Fe^{III}(pzTp)(CN)_3]^-$ anion acts as a monodentate ligand through one of its three cyano groups toward a central $[Ni^{II}$(1-butylimidazole$)_4]^{2+}$ unit, while each $[Ni^{II}$(1-butylimidazole$)_4]^{2+}$ unit is linked to two $[Fe^{III}(pzTp)(CN)_3]^-$ units, yielding a neutral centrosymmetric trinuclear $[Fe^{III}(pzTp)(CN)_3]_2Ni^{II}$(1-butylimidazole$)_4$ molecular structure. Three metal centers were in a linear array with a Fe–Ni–Fe angle of 180°, which is illustrated in Fig. 1. Within the trinuclear cluster, there are one crystallographically independent iron center (Fe1) and one crystallographically independent nickel center (Ni1). The Fe1 center is located in a distorted FeC_3N_3 octahedral coordination environment with three cyano carbon atoms and three nitrogen atoms from the pzTp. The Fe1–C bond lengths are 1.895(5)–1.934(5) Å, and the Fe1–N distances are 1.959(3)–1.981(4) Å, respectively, which is in good agreement with those observed in the related low-spin Fe^{III} tricyanide complexes.[6] The Fe–C≡N linkage is close to linearity with bond angle of 174.7(4)°. Whereas the Ni1 center has a distorted N_6 octahedral coordination surrounding constructed by two cyano nitrogen atoms and four nitrogen atoms from 1-butylimidazole ligands. The Ni1–N distances are 2.074(3)–2.117(4) Å, and the C≡N–Ni

angle (167.9(4)°) slightly deviate from linearity. Selected bond lengths and angles for **1** are listed in Table S1. The intracluster Fe···Ni and Fe···Fe distances are 5.100(1) and 10.201(1) Å, respectively. The nearest intercluster Fe···Ni, Ni···Ni and Fe···Fe distances are 8.730(1), 10.522(1) and 7.681(1) Å, respectively.

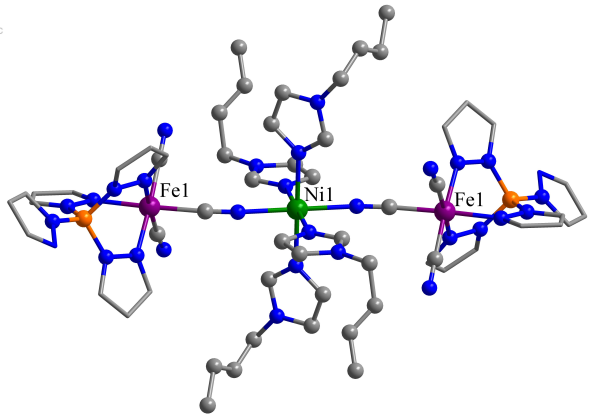

Fig. 1 Crystal structure of **1**, the hydrogen atoms and methanol molecules are omitted for clarity (Fe, violet; Ni, green; C, gray; N, blue; B, orange).

Complex **2** crystallized as a centrosymmetric tetranuclear cluster in the triclinic space group $P\bar{1}$. The crystal structure comprises four components: one tetranuclear square $\{[(Tp^*)Fe^{III}(CN)_3]_2Ni^{II}{}_2(2,2\text{-bipyrimidyl})_4\}^{2+}$ unit, two tetrafluoroborate anions, two methanol molecules, and two solvent water molecules, which is depicted in Fig. 2a. Within the square, each $[Fe^{III}(Tp^*)(CN)_3]^-$ fragment is alternatively connected with two $[Ni(2,2\text{-bipyrimidyl})_2]^{2+}$ units through two of its three cyano groups, forming a centrosymmetric $\{Fe_2(\mu\text{-}CN)_4Ni_2\}$ tetranuclear square structure. The four metal centers are perfectly coplanar in the tetranuclear cluster. The remaining one terminal cyano group is perpendicular to the plane. Each iron center shows a distorted octahedral coordination geometry with three cyano carbon atoms and three nitrogen atoms from the Tp*. The Fe1–C bond lengths are 1.924(8)–1.948(8) Å, and the Fe1–N distances are 1.995(6)–2.011(6) Å, respectively, which are in good accordance with those reported for other low-spin Fe^{III} species.[7] The Fe–C≡N angles fall in the range of 173.6(6)°–178.5(7)°, which are close to linearity. Each nickel center is six-coordinated with two cyano nitrogen atoms and four nitrogen atoms from two bidentate 2,2′-bipyrimidyl ligands, resulting in a distorted NiN_6 octahedral coordination configuration. The Ni1–N distances are in the range of 2.040(7)–2.114(6) Å. The C≡N–Ni1 angles depart from linearity and range between 165.5(6)° and 174.6(6)°. Selected bond lengths and angles for **2** are presented in Table S2. In addition, the hydrogen-bonding interactions are found between the nitrogen atoms of terminal cyano, water molecules, the F atoms of tetrafluoroborate anions, and the C atoms of 2,2-bipyrimidyl ligands, with N···O distances of 3.088(6) Å, C···F distances varying from 2.990(2) to 3.261(2) Å, an C···N distance of 3.508(1) Å, and an C···O distance of 3.200(3) Å (Fig. S1). Furthermore, the neighboring clusters are joined together by intercluster hydrogen bonds, forming a one-dimensional chain structure (Fig. S2). The Fe···Ni separations in the square are 5.086(2) and 5.116(2) Å, and the diagonal Ni···Ni and Fe···Fe separations are 6.887(2) and 7.526(2) Å, respectively. While the nearest intersquare Fe···Ni, Ni···Ni, and Fe···Fe separations are 10.185(3), 9.101(2) and 8.828(2) Å, respectively, indicating that the intersquare magnetic interactions are very weak.

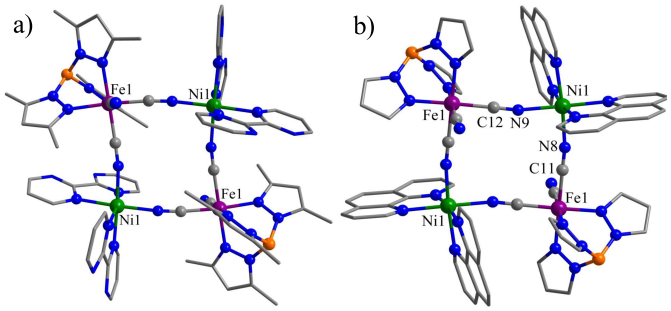

Fig. 2 Crystal structure of **2** (a) and **3** (b). The anions, hydrogen atoms, methanol and water molecules are omitted for clarity (Fe, violet; Ni, green; C, gray; N, blue; B, orange).

The crystal structure of **3** is similar to that of **2**. It is composed of one tetranuclear square $\{[(Tp)Fe^{III}(CN)_3]_2Ni^{II}{}_2(1,10\text{-phenanthroline})_4\}^{2+}$ unit, two solvent water molecules, and two perchlorate anions (Fig. 2b). The tetranuclear square unit consists of two $[Fe^{III}(Tp)(CN)_3]^-$ units and two $[Ni^{II}(1,10\text{-phenanthroline})_2]^{2+}$ units. The two moieties bridged each other through cyano groups, yielding a centrosymmetric tetranuclear square structure. In the square, the four metal ions are coplanar. The coordination environment of each metal ion is a distorted octahedral geometry. The six coordination sites of the iron center are occupied by three nitrogen atoms from Tp and three cyano carbon atoms. The Fe1–C bond lengths are 1.910(5)–1.928(6) Å, and the Fe1–N distances are 1.961(3)–1.972(4) Å, respectively, which is characteristic of low-spin Fe^{III} ion. These Fe1–C and Fe1–N bond lengths are very close to those found in the related tetranuclear complexes. The Fe–C≡N angles are almost linear with bond angles of 177.9(5)–179.5(4)°. While the nickel center is coordinated to two cyano nitrogen atoms and four nitrogen atoms from two bidentate 1,10-phenanthroline ligands. The Ni1–N bond lengths range between 2.041(4) and 2.110(4) Å, being similar to those seen in **2**. The values of the C≡N–Ni angles are 167.2(4)°–170.3(3)°. Selected bond lengths and angles for **3** are listed in Table S3. Moreover, there exists π–π stacking interactions between the adjacent pyrazolyl rings, and aromatic rings of adjacent 1,10-phenanthroline ligands. The closest separation of pyrazolyl rings is 3.512(1) Å, while the closest separation of aromatic rings is 3.508(1) Å (Fig. S3). Furthermore, the hydrogen-bonging interactions are found between water molecules and carbon atoms, with an C···O distance of 3.460(4) Å. The Fe···Ni distances within the square are 5.081(1) Å, and the diagonal Ni···Ni and Fe···Fe distances are 7.104(1) and 7.266(1) Å, respectively. While the shortest intersquare Fe···Ni, Ni···Ni,

and Fe···Fe distances are 9.827(1), 8.690(1) and 7.609(1) Å, respectively.

Magnetic studies

The temperature-dependent magnetic susceptibilities (χ) of **1** were measured under 1000 Oe in the temperature range of 2–300 K (Fig. 3a). The χT value at 300 K was 2.57 cm^3 mol^{-1} K per Fe_2Ni unit, which is larger than the spin–only value for two magnetically isolated low–spin Fe^{III} ions (S = 1/2, g = 2.0) and one magnetically isolated high–spin Ni^{II} ion (S = 1/2, g = 2.0). As the temperature decreased, the χT value gradually increased to a maximum value of 6.9 cm^3 mol^{-1} K at 7.5 K, this behavior displays that ferromagnetic interactions dominates in **1**. The maximum value of 6.9 cm^3 mol^{-1} K is larger than the theoretical value for the magnetically isolated trinuclear compounds with S = 2. This may come from intermolecular ferromagnetic interactions. Below 7.5 K, the χT value sharply decreases and reaches a value of 5.22 cm^3 mol^{-1} K at 2 K, which could be attributed to the zero–field splitting and/or weak intercluster antiferromagnetic interactions.[8] In the temperature range of 10–300 K, the magnetic susceptibility data are fitted to the Curie–Weiss law with a Curie constant C of 2.54 cm^3 mol^{-1} K and a Weiss constant θ of 6.14 K. The positive Weiss constant further confirms the ferromagnetic behavior of **1**. Moreover, the ferromagnetic behavior is also supported by the field-dependent magnetization measured at 1.8 K (Fig. S4). As the applied magnetic field increased, the magnetization increases first rapidly, and then reaching a maximum value of 4.2 $N\beta$ at 50 kOe, which is close to the saturated value for two low-spin Fe^{III} ions and one high-spin Ni^{II} ion. It should be noted that no hysteresis is observed at 1.8 K.[9] In addition, the plots of zero field-cooled magnetization (ZFCM) and field-cooled magnetization (FCM) under a field of 100 Oe show irreversibility below 4.5 K, indicating the occurrence of spontaneous magnetization at low temperatures (Fig. S5).

To investigate the dynamics of the magnetization of **1**, the alternating current (ac) magnetic susceptibility was measured as a function of both temperature and frequency (Fig. 3b). The in-phase (χ') and out-of-phase (χ'') showed apparent frequency dependency, as was observed in related SMMs. Meanwhile, there are obvious peaks in the χ' and χ'' data from 4 to 10 K, which moved to higher temperature with increasing frequency. The frequency-dependent behavior precluded a three-dimensional ordering. Moreover, the parameter Φ ($\Phi = (\Delta T_p/T_p)/\Delta(\log\upsilon)$, Where υ is the frequency and T_P is the peak temperature of χ'') was used to distinguish between glass and superparamagnetism. The calculated value of 0.13 is out of the range for spin-glass but lies in the expected range for a superparamagnet, and thus rules out the possibility of spin-glass behavior. On the basis of these data, the relaxation times were estimated and fitted to Arrhenius law of $\tau = \tau_0\exp(\Delta/k_BT)$ ($\tau^{-1} = 2\pi\upsilon$), where τ, τ_o, υ and Δ/k_B represent relaxation time, pre-exponential factor, frequency and relaxation energy barrier, respectively. The best fitting give a pre-exponential factor of $\tau_o = 1.03\times10^{-9}$ s and a corresponding relaxation energy barrier of Δ/k_B = 106.2 K (Fig. 3c). The above results suggests that the intermolecular magnetic interactions did not suppress the spin relaxation of the molecule. However, the energy barrier is higher than similar types of SMM due to intermolecular ferromagnetic interactions. These values are in good agreement with those reported values for typical SMMs (usually > 10^{-12} s).[10] This analysis demonstrates that the presence of a SMMs behavior in **1**.

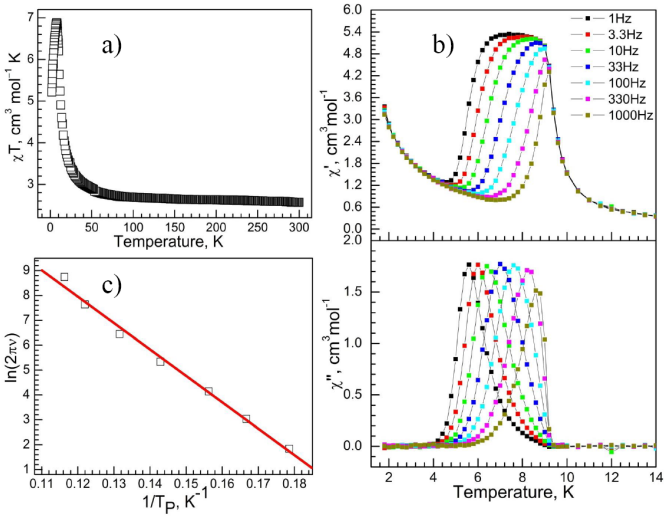

Fig. 3 a) Temperature-dependent magnetic susceptibilities of **1** in the temperature range of 2–300 K under an applied field of 1000 Oe. b) Temperature dependence of the real part and the imaginary part of the ac susceptibility of **1** in a zero dc field and a 3.5 Oe ac field. c) The plot of $\ln(2\pi\upsilon)$ versus T_P^{-1} of **1**, where υ is the frequency and T_P is the peak temperature of χ''. The solid line represents the least-squares fit of the experimental data to the Arrhenius equation.

The temperature-dependent magnetic susceptibilities of **2** and **3** are presented in Fig. 4. At 300K, the χT products were 3.54 and 3.63 cm^3 mol^{-1} K for **2** and **3**, respectively. From 300 to 70 K, the χT product is practically constant and increases rapidly to a maximum value of 13.89 and 6.55 cm^3 mol^{-1} K at 7 K for **2** and 9 K for **3,** respectively. Such a magnetic behavior indicates that the presence of a intramolecular ferromagnetic coupling between Fe^{III} and Ni^{II} ions through the cyano-bridges. The maximum value of 13.89 cm^3 mol^{-1} K for **2** is larger than the theoretical value for the magnetically isolated tetranuclear compounds with S = 3. This may come from intermolecular ferromagnetic interactions. As the temperature further decreased, the χT product abruptly decreases to 10.23 and 3.32 cm^3 mol^{-1} K for **2** and **3** at 2 K, respectively. This may be due to the presence of the zero–field splitting and/or weak intercluster antiferromagnetic interactions. The best fitting of the magnetic susceptibility data with the Curie–Weiss law in 20–300 K for **2** and **3**, respectively, giving C = 3.49 cm^3 mol^{-1} K and θ = 6.62 K for **2**, and C = 3.50 cm^3 mol^{-1} K and θ = 4.72 K for **3**. The positive Weiss constant further indicates the ferromagnetic coupling between the Fe^{III} and Ni^{II} ions. In addition, the ferromagnetic behavior is also in accordance with the field-dependent magnetization of **2** and **3** at 1.8 K (Fig. S6).

As the applied magnetic field increased, the isothermal magnetization increases linearly at low fields, reaching a value of 6.32 and 6.46 *Nβ* for **2** and **3**, respectively, at 50 kOe, which is close to the theoretical value for two low-spin Fe^{III} ions and two high-spin Ni^{II} ions. A magnetizaiton hysteresis loop is observed at 1.8 K (Fig. 4 Inset) with values of the remnant magnetization (*Mr*) and coercive field (*Hc*) of 1.0 *Nβ* and 1200 Oe for **2**, and 0.12 *Nβ* and 400 Oe for **3**, respectively. It should be noted that the coercive field of **2** is much larger than that in **3**. In addition, the plots of ZFCM and FCM under a field of 100 Oe (Figure S7) show irreversibility below 4.6 K for **2**, and below 4.0 K for **3**, respectively, indicating the occurrence of spontaneous magnetization at low temperatures.

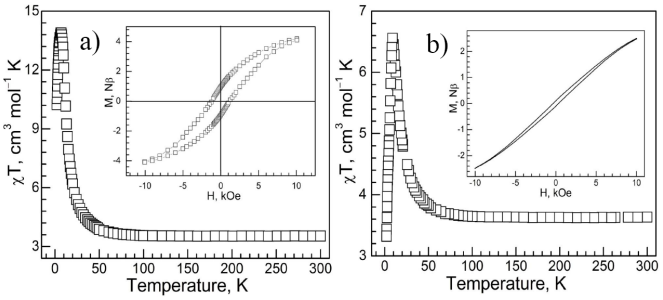

Fig. 4 Temperature-dependent magnetic susceptibilities of **2** (a) and **3** (b) in the temperature range of 2–300 K under an applied field of 1000 Oe. Inset: Hysteresis loop of **2** (a) and **3** (b) at 1.8 K.

To probe the dynamics of the magnetization of **2** and **3**, the ac magnetic susceptibility was measured under a 3.5 Oe ac field (Fig. 5). The frequency dependency characteristics of χ' and χ'' can be observed below 5 K for **2**, and below 4 K for **3**, respectively. Meanwhile, the peaks in the χ' and χ'' data are shifted to higher temperature with increasing frequency. The frequency-dependent characteristics rules out a three-dimensional ordering, and is consistent with slow magnetic relaxation exhibited by a SMM or spin-glass. However, the value of calculated Φ is 0.11 for **2**, and 0.17 for **3**, respectively, which lies in the range expected for a SMM, and thus eliminate the possibility of spin-glass behavior. The value of estimated τ_o is 2.34×10^{-11} s for **2** and 6.42×10^{-9} s for **3**, and the corresponding relaxation energy barrier Δ/k_B is 64.3 K for **2**, and 24.5 K for **3**, respectively (Fig. 5 inset). These values are in good accordance with those reported values for typical SMMs (usually > 10^{-12} s), which indicates **2** and **3** exhibit SMMs behavior.

Investigation of the magnetic properties of the three cyano-bridged heterometallic Fe^{III}–Ni^{II} complexes reveals the ferromagnetic interactions between the Fe^{III} and Ni^{II} ions, which is easily rationalized in terms of the strict orthogonality of the magnetic orbitals of the low-spin Fe^{III} and Ni^{II} ions.[11–13] In comparison to Tp*, the steric hinder between Tp and ancillary ligand in **3** is smaller than that of **2**, so there is shorter distances between the intercluster metal ions, and there exists π–π stacking interactions and hydrogen-bonding interactions in **3**. While in **2**, only weak hydrogen-bonding interactions are observed. The dynamic susceptibility measurements are clearly illustrative for the SMM behavior. The intramolecular ferromagnetic coupling is rather visible as main feature, while low temperature details are assignable to local anisotropy on Ni(II) sites and possibly intermolecular interactions. The slow relaxation of the magnetization is not suppressed by the intercluster interactions. Although many Fe–Ni polynuclear complexes have been reported, few of them show magnetic hysteresis.[14] These results indicate that the enhancement of the steric hinder to minimize the intercluster magnetic interactions and introduction of proper ancillary ligand and building block to tune the magnetic interactions may play an important role in the formation of SMMs.

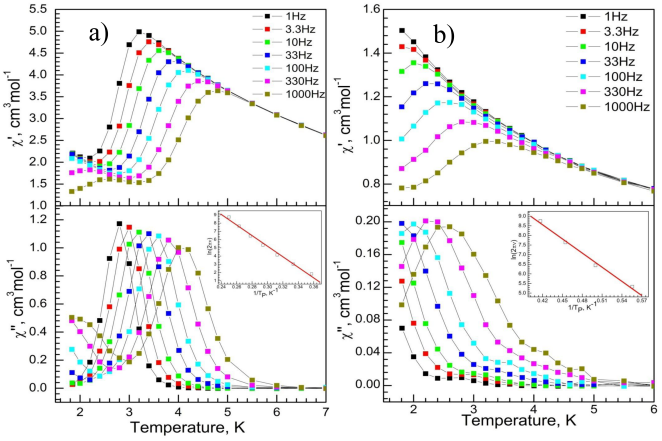

Fig. 5 Temperature-dependent of the real part and the imaginary part of the ac susceptibility for **2** (a) and **3** (b) in a zero dc field and a 3.5 Oe ac field. Inset: the plot of $\ln(2\pi\upsilon)$ versus T_P^{-1}, Where T_P is the peak temperature of χ'', the solid line represents the least-squares fit of the experimental data to the Arrhenius equation.

Conclusions

In conclusion, we have synthesized three new cyano-bridged mixed-valence heterometallic Fe^{III}–Ni^{II} complexes. The magnetic studies demonstrate that **1**–**3** exhibit ferromagnetic interactions between Fe^{III} and Ni^{II} ions, and SMMs behavior. The present work focuses on taking advantage of the steric hindrance effect to decrease the intermolecular interactions to obtain SMMs.

Experimental

Materials and methods

All organic solvents and material used for synthesis were of reagent grade and used without further purification. $Bu_4N[Fe(pzTp)(CN)_3]$, $Bu_4N[Fe(Tp^*)(CN)_3]$ and $Bu_4N[Fe(Tp)(CN)_3]$ were prepared according to the literature method.[15] Elemental analyses (C, H, and N) were carried out on an Elementar Vario EL III analyzer. Magnetic measurement was performed on a Quantum Design SQUID (MPMS XL-7) magnetometer. The magnetic susceptibilities of microcrystalline samples of **1**-**3** were measured, the powder X-ray diffraction analysis confirmed their purity (Figure S8). A

correction was made for the diamagnetic contribution prior to data analysis.

Synthesis of $[(pzTp)Fe^{III}(CN)_3]_2Ni^{II}(1\text{-butylimidazole})_4\cdot CH_3OH$ (1)

A 6.0 mL aqueous solution of $Ni(BF_4)_2\cdot 6H_2O$ (0.05 mmol) was placed at the bottom of a test tube, a mixture of methanol and water (1:1, v/v, 6 mL) was gently layered on the top of the solution, and then a 6.0 mL methanol solution of $Bu_4N[Fe(pzTp)(CN)_3]$ (0.1 mmol) and 1-butylimidazole (0.2 mmol) was carefully added as the third layer. Six weeks later, red crystals appeared and were collected and dried in air after quickly being washed with water. Yield: 62% based on $Ni(BF_4)_2\cdot 6H_2O$. Anal. calcd (%) for $C_{59}H_{76}B_2NiFe_2N_{30}O$: C, 50.02; H, 5.38; N, 29.59; Found (%): C, 50.14; H, 5.42; N, 29.73.

Synthesis of $[(Tp^*)Fe^{III}(CN)_3]_2Ni_2^{II}(2,2\text{-bipyrimidyl})_4\cdot 2BF_4\cdot 2CH_3OH\cdot 2H_2O$ (2)

A 3.0 mL methanol solution of $Bu_4N[Fe(Tp^*)(CN)_3]$ (0.1 mmol) and 2,2-bipyrimidyl (0.1 mmol) was placed at the bottom in one side of an H-shaped tube, and a 3.0 mL aqueous solution of $Ni(BF_4)_2\cdot 6H_2O$ (0.05 mmol) was introduced into the other side. Then, 12 mL of methanol was layered over the solutions on both sides to provide a diffusion pathway. Crystallization required ten weeks, Yield: 55% based on $Ni(BF_4)_2\cdot 6H_2O$. Anal. calcd (%) for $C_{70}H_{80}B_4F_8Fe_2N_{34}Ni_2O_4$: C, 44.63; H, 4.23; N, 25.38; Found (%): C, 44.58; H, 4.28; N, 25.25.

Synthesis of $[(Tp)Fe^{III}(CN)_3]_2Ni_2^{II}(1,10\text{-phenanthroline})_4\cdot 2ClO_4\cdot 2H_2O$ (3)

Complex **3** was prepared in the same way as for **2**, except using $Bu_4N[Fe(Tp)(CN)_3]$ (0.1 mmol) and 1,10-phenanthroline (0.1 mmol) to replace $Bu_4N[Fe(Tp^*)(CN)_3]$ and 2,2-bipyrimidyl, respectively. Red crystals appeared after nine weeks, Yield: 52% based on $Ni(BF_4)_2\cdot 6H_2O$. Anal. calcd (%) for $C_{72}H_{56}B_2Cl_2Fe_2N_{26}Ni_2O_{10}$: C, 48.79; H, 3.14; N, 20.78; Found (%): C, 48.94; H, 3.19; N, 20.61.

Crystallography

The data were collected at a temperature of 296 K on a Bruker Smart APEX II X–diffractometer equipped with graphite monochromated *M*o–*K*α radiation (λ = 0.71073 Å) using the SMART and SAINT programs. The structure was solved by direct methods and refined on F^2 by using full-matrix least-squares methods with *SHELXTL*–97.[16] For complexes **1**–**3**, all non-hydrogen atoms and part solvent water molecules were refined anisotropically. Hydrogen atoms of the organic ligands were generated geometrically and fixed isotropic thermal parameters. The crystal data and details of structure refinement for complexes 1-3 are summarized in Table S4.

Acknowledgements

This work was partly supported by the NSFC (Grants 21201028, 91122031, 21421005, and 21322103) and the Fundamental Research Funds for the Central Universities, China.

Notes and references

[a] State Key Laboratory of Fine Chemicals, Dalian University of Technology, Dalian, 116024, China. E-mail: liutao@dlut.edu.cn.

† Electronic Supplementary Information (ESI) available: Figures S1–S6, Tables S1–S3 and CCDC number of **1** (1012525), **2** (1012526) and **3** (1012527). X-ray crystallographic file in CIF format for **1**–**3** are provided. See DOI: 10.1039/b000000x/

1 (a) M. N. Leuenberger and D. Loss, *Nature*, 2001, **410**, 789; (b) G. Lorusso, M. A. Palacios, G. S. Nichol, E. K. Brechin, O. Roubeau and M. Evangelisti, *Chem. Commun.*, 2012, **48**, 7592; (c) F. Troiani and M. Affronte, *Chem. Soc. Rev.*, 2011, **40**, 3119.

2. (a) J. Černák, M. Orendáč, I. Potočňák, J. Chomič, A. Orendáčová, J. Skoršepa and A. Feher, *Coord. Chem. Rev.*, 2002, **224**, 51; (b) K. R. Dunbar and R. A. Heintz, *Prog. Inorg. Chem.*, 1997, **45**, 283; (c) K. S. Pedersen, J. Bendix and R. Clerac, *Chem. Commun.*, 2014, **50**, 4396; (d) M. Verdaguer, A. Bleuzen, V. Marvaud, J. Vaissermann, M. Seuleiman, C. Desplanches, A. Scuiller, C. Train, R. Garde, G. Gelly, C. Lomenech, I. Rosenman, P. Veillet, C. Cartier and F. Villain, *Coord. Chem. Rev.,* 1999, **190–192**, 1023.

3. (a) O. Kahn and C. J. Martinez, *Science*, 1998, **279**, 44; (b) J. F. Letard, J. A. Real, N. Moliner, A. B. Gaspar, L. Capes, O. Cador and O. Kahn, *J. Am. Chem. Soc.*, 1999, **121**, 10630; (c) A. Mondal, Y. Li, P. Herson, M. Seuleiman, M. L. Boillot, E. Riviere, M. Julve, L. Rechignat, A. Bousseksou and R. Lescouezec, *Chem. Commun.*, 2012, **48**, 5653; (d) M. Nihei, M. Ui, M. Yokota, L. Q. Han, A. Maeda, H. Kishida, H. Okamoto and H. Oshio, *Angew. Chem. Int. Ed.*, 2005, **44**, 6484.

4. (a) D. Gatteschi and R. Sessoli, *Angew. Chem. Int. Ed.*, 2003, **42**, 268; (b) S. Wang, X. H. Ding, J. L. Zuo, X. Z. You and W. Huang, *Coord. Chem. Rev.*, 2011, **255**, 1713.

5. (a) L. M. C. Beltran and J. R. Long, *Acc. Chem. Res.*, 2005, **38**, 325; (b) S. Kanegawa, S. Karasawa, M. Maeyama, M. Nakano and N. Koga, *J. Am. Chem. Soc.*, 2008, **130**, 3079; (c) X.-Y. Wang, C. Avendano and K. R. Dunbar, *Chem. Soc. Rev.*, 2011, **40**, 3213; (d) D. Zhang, H. Wang, Y. Chen, Z. H. Ni, L. Tian and J. Jiang, *Inorg. Chem.*, 2009, **48**, 11215; (e) L. M. Toma, C. Ruiz-Perez, J. Pasan, W. Wernsdorfer, F. Lloret and M. Julve, *J. Am. Chem. Soc*., 2012, **134**, 15265.

6. (a) D. Li, R. Clérac, G. Wang, G. T. Yee and S. M. Holmes, *Eur. J. Inorg. Chem.*, 2007, 1341; (b) S. Wang, J. L. Zuo, H. C. Zhou, Y. Song, S. Gao and X. Z. You, *Eur. J. Inorg. Chem.*, 2004, 3691.

7. (a) E. Pardo, M. Verdaguer, P. Herson, H. Rousseliere, J. Cano, M. Julve, F. Lloret and R. Lescouezec, *Inorg. Chem.*, 2011, **50**, 6250; (b) D. P. Dong, Y. J. Zhang, H. Zheng, P. F. Zhuang, L. Zhao, Y. Xu, J. Hu, T. Liu and C. Y. Duan, *Dalton. Trans.*, 2013, **42**, 7693.

8. D. Visinescu, L. M. Toma, J. Cano, O. Fabelo, C. Ruiz-Perez, A. Labrador, F. Lloret and M. Julve, *Dalton. Trans.*, 2010, **39**, 5028.

9. (a) J. J. Sokol, A. G. Hee and J. R. Long, *J. Am. Chem. Soc.*, 2002, **124**, 7656; (b) Z. G. Gu, W. Liu, Q. F. Yang, X. H. Zhou, J. L. Zuo

and X. Z. You, *Inorg. Chem.*, 2007, **46**, 3236; (c) Y. Z. Zhang, U. P. Mallik, N. P. Rath, R. Clerac and S. M. Holmes, *Inorg. Chem.*, 2011, **50**, 10537.

10. W. Liu, C. F. Wang, Y. Z. Li, J. L. Zuo and X. Z. You, *Inorg. Chem.*, 2006, **45**, 10058.
11. (a) C. F. Wang, W. Liu, Y. Song, X. H. Zhou, J. L. Zuo and X. Z. You, *Eur. J. Inorg. Chem.*, 2008, 717; (b) A. Panja, P. Guionneau, R. Jeon Ie, S. M. Holmes, R. Clerac and C. Mathoniere, *Inorg. Chem.*, 2012, **51**, 12350; (c) Y. Z. Zhang, U. P. Mallik, R. Clérac, N. P. Rath and S. M. Holmes, *Polyhedron.*, 2013, **52**, 115.
12. (a) Z. G. Gu, Q. F. Yang, W. Liu, Y. Song, Y. Z. Li, J. L. Zuo and X. Z. You, *Inorg. Chem.*, 2006, **45**, 8895; (b) N. Hoshino, Y. Sekine, M. Nihei and H. Oshio, *Chem. Commun.*, 2010, **46**, 6117; (c) A. Rodríguez-Diéguez, R. Kivekäs, R. Sillanpää, J. Cano, F. Lloret, V. McKee, H. Stoeckli-Evans and E. Colacio, *Inorg. Chem.*, 2006, **45**, 10537; (d) S. Wang, J. L. Zuo, H. C. Zhou, Y. Song and X. Z. You, *Inorg. Chim. Acta.*, 2005, **358**, 2101; (e) D. Wu, Y. Zhang, W. Huang and O. Sato, *Dalton. Trans.*, 2010, **39**, 5500.
13. J. N. Rebilly and T. Mallah, *Struct. bond.*, 2006, **122**, 103.
14. J. Kim, S. Han, K. I. Pokhodnya, J. M. Migliori and J. S. Miller, *Inorg. Chem.*, 2005, **44**, 6983.
15. (a) R. Lescouezec, J. Vaissermann, F. Lloret, M. Julve and M. Verdaguer, *Inorg. Chem.*, 2002, **41**, 5943; (b) D. F. Li, S. Parkin, G. B. Wang, G. T. Yee and S. M. Holmes, *Inorg. Chem.*, 2006, **45**, 1951; (c) D. F. Li, R. Clerac, S. Parkin, G. B. Wang, G. T. Yee and S. M. Holmes, *Inorg. Chem.*, 2006, **45**, 5251.
16. G. M. Sheldrick, SHELXL-97, *Program for X-ray Crystal Structure Refinement*, University of Göttingen, Göttingen, 1997.